Molecular Squares, Rectangles, and Corners: Ground-State Electronic Structure and Configurational Properties

Donald E. Ellis,*[,†,‡,§] Ljubomir Miljacic,[†] Bin Deng,[§] Ming Jiang,[†,||] Lev Sarkisov,[⊥] and Randall Q. Snurr[‡,⊥]

Department of Physics & Astronomy, Institute of Environmental Catalysis, Department of Chemistry, and Department of Chemical Engineering, Northwestern University, Evanston, Illinois 60208, and Department of Physics, Yantai University, People's Republic of China

Received June 7, 2005. Revised Manuscript Received September 28, 2005

A recently developed class of molecular squares based on octahedral $ReCl(CO)_3R_2$ cornerposts has until now lacked a detailed theoretical description. We present an analysis of electronic structure of five of the simplest squares, rectangles, and related fragments; that is, those with pyrazine and bipyridine walls. We further consider a square containing Zn−porphyrin walls. The derived electronic charge distributions reveal bonding structure and spectral features of the class. We show that the analysis of conformational preferences can be greatly simplified by using a "piecewise" strategy, which enables us to make several generic statements about conformations of this class of macromolecules. To further illustrate advantages of this approach, we find the origin of metastability of the planar conformation of the bipyridine square.

I. Introduction

Rectangular macromolecules built up from $[ReCl(CO)_3R_2]$ "corner posts" with linking macrocycle "walls" self-assemble into hydrophobic extended thin film and crystalline structures with distinctive porosity. As such, these "molecular squares and boxes" show potential for size-selective filtration and separation in the form of supported membranes, complementary to that of hydrophilic porous structures such as zeolites. Further, substitution of metal complexes into walls or as bridging elements within the boxes can provide catalytic sites with both chemical and geometric control of the environment of incoming molecules.[1−8] Such systems can be viewed as biologically inspired enzymes, with a degree of control in electronic and steric structure difficult to achieve in naturally occurring systems. By synthesis, characterization, and theoretical analysis of such artificial systems, we also hope to achieve a more profound understanding of structure/function relations of real enzymes.

In this work we present a theoretical analysis of ground-state electronic structure of several of the simplest squares and related fragments; that is, those with pyrazine (pz) and bipyridine (bpy) walls. We further consider a square whose walls contain a zinc porphyrin, which serves as a prototype for a structurally constrained catalytic system. The electronic charge distributions give insight into bonding structures and spectral distributions generic to the series. They will be used in the future as guidance in construction of force fields, to be used in molecular dynamic simulations of thin films and their interaction with diffusing molecules. In the present context, we analyze the ground-state charge distribution and densities of states (DOS) of molecules whose structure has been determined by X-ray diffraction or can be inferred from analogous compounds.

A limited structural investigation, varying a few critical parameters, is carried out to verify sensitivity of electronic density and mechanical response to geometry. The knowledge of conformations of these macromolecules is important in developing synthesis and processing strategies which will result in ordered and oriented macromolecular structures. Especially attractive is the prospect of understanding generic conformational characteristics of the group and getting insight about their origin. This would lead to design principles for controlling structure. A "piecewise" approach to torsion-controlled structure is shown here to be both applicable and effective for this class of materials.

II. Theoretical Methodology

Density functional theory (DFT) is our method of choice in determining electronic density ρ and derived properties of the ground state of molecules and solids.[9−12] Contour maps of the density, examination of bond distributions, projection onto local DOS, and atomic orbital populations provide much insight into bonding mechanisms and hints about reactivity.

* To whom correspondence should be addressed. E-mail: don-ellis@northwestern.edu.
[†] Department of Physics & Astronomy, Northwestern University.
[‡] Institute of Environmental Catalysis, Northwestern University.
[§] Department of Chemistry, Northwestern University.
[||] Yantai University.
[⊥] Department of Chemical Engineering, Northwestern University.

(1) Fujita, M.; Yakazi, J.; Ogura, K. *J. Am. Chem. Soc.* **1990**, *112*, 5645.
(2) Fujita, M.; Yakazi, J.; Ogura, K. *Tetrahedron Lett.* **1991**, *32*, 5589.
(3) Fujita, M.; Sasaki, O.; Mitsuhashi, T.; Fujita, T.; Yagazi, J.; Yamaguchi, K.; Ogura, K. *J. Chem. Soc., Chem. Commun.* **1996**, 1535.
(4) Stang, P.; Olenyuk, B. *Acc. Chem. Res.* **1997**, *30*, 502.
(5) Slone, R. V.; Yoon, D. I.; Calhoun, R. M.; Huff, J. T. *J. Am. Chem. Soc.* **1995**, *117*, 11813.
(6) Slone, R. V.; Hupp, J. T.; Stern, C. L.; Albrecht-Schmitt, T. E. *Inorg. Chem.* **1996**, *35*, 4096.
(7) Slone, R. V.; Hupp, J. T. *Inorg. Chem.* **1997**, *36*, 5422.
(8) Leung, W.-H.; Cheng, J. Y. K.; Hun, T. S. M.; Che, C.-M.; Wong, W.-T.; Cheung, K. K. *Organometallics* **1996**, *15*, 1497.
(9) Ellis, D. E., Ed. *Electronic Density Functional Theory of Molecules, Clusters, and Solids*; Kluwer: Dordrecht, 1995.
(10) Seminario, J. M., Ed. *Recent Developments and Applications of Density Functional Theory*; Elsevier: Amsterdam, 1996.

10.1021/cm051214o CCC: $33.50
Published on Web 01/14/2006

At the most basic level, Mulliken atomic orbital populations and net atomic charges provide a comparative basis for interpreting self-consistent electronic configurations in the set of molecules studied. It is well-known that Mulliken populations do not have absolute significance as a result of their dependence upon basis; however, they are quite valuable in a comparative sense. Volume integrations are also subject to choice of integration region, and quantitative interpretation of density maps is not trivial. Thus, comparisons based upon several different "points of view" are highly useful. Mulliken populations and atomic charges in a compact basis generally compare well with chemical expectations. The diffuse functions of a variationally superior basis can often lead to unrealistic projected Mulliken atomic charges, because diffuse functions assigned to one atom may overlap considerably onto nearby atomic sites. In such cases volume integration provides a more reliable measure of charge distribution localization.

Partial densities of states (PDOS), $N_p(E)$, describe the spectral distribution of specific atomic orbital character; the atom-selected and atomic-orbital-selected PDOS give us a direct measure of the bonding characteristics in the local environment. PDOS were calculated by weighting individual energy levels according to the Mulliken atomic orbital populations D_p of the desired species and broadening to obtain continuous curves

$$N_p(E) = \sum_i D_p(\epsilon_i)\, L(E - \epsilon_i, \sigma) \qquad (1)$$

where $L(\epsilon, \sigma)$ is a Lorentzian line shape of width σ. We choose the Fermi energy (E_F) as the zero point of the energy axis.

The charge and bond order matrix Q_{ij} describes the charge distribution of occupied states over orbital pairs (i, j). Summing over orbitals belonging to particular atoms, we obtain the shared charge between atom pairs (p, q). A further approach to interpreting bonding is found in Bader's topological theory of atoms in molecules.[12] Here the charge density at a bond critical point can be taken as an index of bond type and strength. The matrix bond orders and bond critical point densities provide a complementary and mutually reinforcing picture of interatomic charge sharing. The Q-matrix approach is most useful for interpretation in compact, highly localized bases. However, the critical densities are, in principle, basis independent.

For this work we have used two different DFT computational codes. The Mulliken charges, PDOS, and bond order analysis are based upon expansions of the molecular self-consistent eigenvectors within a basis set of numerical atomic orbitals (NAOs), which are adapted to the molecular potential, all within the discrete variational method[9] (DVM). The NAOs used in the expansions are Re 1s,...,5p,5d,6s,6p, Cl 1s,...,3d,4s,4p, O 1s,2s2p,3s,3p, N 1s,2s,2p,3s,3p, C 1s,2s,2p,3s,3p, and H 1s, referred to hereafter as basis B2. Compact basis calculations were also made, omitting the ligand 3s,3p NAOs, referred to hereafter as basis B1. Core levels consisting of Re [1s,...,4d], Cl [1s,...,2p], O [1s], N [1s], and C [1s] were treated in the "frozen core" approximation; valence levels were maintained orthogonal to the core during self-consistent field (SCF) iterations.

For the analysis of conformational properties, we employed the Amsterdam density functional (ADF) program,[13] because of its advanced capability in performing geometry optimizations. Here, we used a large basis set of Slater-type orbitals containing polarized triple-ζ functions for Re and Zn and polarized double-ζ bases for other atoms, with the frozen core approximation the same as in the DVM approach. The precision of numerical integration was set high to reduce the dispersion of total-energy data.[14,15]

Concerning the level of reliability or "error bars" that can be established for DFT (in general, or for one of its many implementations in particular), the answer depends on the physical property examined.[9−15] It is generally established that the ground-state charge density is of similar accuracy to Hartree−Fock, that is, $\sim$ 1% error compared to the best available X-ray diffraction data. For chemical binding energies and bond lengths, both generalized gradient approximation (GGA) and the hybrid DFT/HF B3LYP exchange-correlation functionals generally perform better than the simplest local density approximation (LDA). However, this improvement comes at the expense of other properties, for example, magnetic moments and hyperfine fields. One can obviously find pathological cases in any methodology, so we may only speak of averages of sets of atoms, molecules, and solids. Efforts are ongoing to improve DFT treatment of exchange-correlation interactions; however, for present purposes of ground-state charge density and bonding analysis, a large body of experience suggestions that the LDA scheme is quite sufficient. In our previous work,[16] we have concluded that, in terms of conformational preferences, the GGA level of theory yields the same information as the simpler LDA scheme.

III. Charge Distributions and Densities of States

A. Cornerpost Unit. *1. Background.* The Re-cornerpost unit, with sixfold quasi-octahedral coordination, $Re(CO)_3ClR_2$, where R = pz, bpy, presents a nitrogen bond to the metal. If we consider the neutral ground configuration Re^0 $5d^56s^2$ it would appear natural that each metal valence electron would contribute to a double bond linking each ligand. The excited state properties of Re(I) pseudo-octahedral complexes have been extensively studied experimentally,largely because of the existence of long-lived luminescent triplet states with potential use as biophysical probes.[17] Qualitative models may portray the metal state as Re(I) or monovalent Re^{1+} $5d^66s^0$, based upon ligand-field arguments, and in analogy to the

(11) Parr, R. G.; Yang, W. *Density Functional Theory of Atoms and Molecules*; Oxford University Press: New York, 1989.
(12) Bader, R. F. W. *Atoms in Molecules: A Quantum Theory*; Oxford University Press: New York, 1990.
(13) te Velde, G.; Bickelhaupt, F. M.; Baerends, E. J.; Fonseca Guerra, C.; van Gisbergen, S. J. A.; Snijders, J. G.; Ziegler, T. *J. Comput. Chem.* **2001**, *22*, 931.
(14) Boerrigter, P. M.; te Velde, G.; Baerends, E. J. *Int. J. Quantum Chem.* **1996**, *33*, 4096.
(15) te Velde, G.; Baerends, E. J. *J. Comput. Phys.* **1992**, *99*, 84.
(16) Miljacic, L.; Sarkisov, L.; Ellis, D. E.; Snurr, R. Q. *J. Chem. Phys.* **2004**, *121*, 7228.
(17) Vogler, A.; Kunkely, H. *Coord. Chem. Rev.* **2000**, *200−202*, 991.

Table 1. Selected Net Atomic Charges for Molecular Squares and Rectangles According to Mulliken Populations Derived from a Compact NAO Basis (Basis B1, See Text) and Corresponding Volume Integrations[a]

	$[Re(CO)_3(\mu\text{-pz})Cl]_4$		$[Re(CO)_3(\mu\text{-bpy})Cl]_4$		$[Re(CO)_3(Zn-pyridyl-porphyrine)]_4$		$[Re_2(CO)_6(\mu\text{-bpy})(\mu,\mu\text{-bi-pyrimidine})]_2$	
	Mull.	vol.	Mull.	vol.	Mull.	vol.	Mull.	vol.
Re	1.65	3.46	1.63	3.17	1.51	2.46	1.97	3.52
Zn					1.88			
Cl	−0.37	−0.11	−0.63	−0.35	−0.38	−0.23		
O	−0.56	−0.07	−0.59	0.08	−0.85	0.09	−0.55	0.05
N_1							−0.52	−0.04
N_2	−0.47	−0.05	−0.53	−0.08	−0.82	−0.04	−0.57	−0.16
C_1[b]	0.14	−0.79	0.26	−0.79	0.23	−0.5	0.16	−0.74
C_2[c]	−0.24	0.46	−0.24	0.49	0.35	0.29	−0.23	0.48

[a] A Fermi function $\{\exp[\zeta(r - R_0) + 1\}^{-1}$ roll-off with radius $R_0 = 1.4a_0$ and tail parameter $\zeta = 2$ was used to define overlapping atomic volumes for integration. [b] Carbon atom in carbonyl group. [c] Carbon atoms on the bridging ligands, averaged over unequivalent sites.

Table 2. Selected Net Atomic Charges for Molecular Squares and Rectangle According to Mulliken Populations Derived from an Extended Atomic Orbital Basis (Basis B2, See Text) and Corresponding Volume Integrations[a]

	$[Re(CO)_3(\mu\text{-pz})Cl]_4$		$[Re(CO)_3(\mu\text{-bpy})Cl]_4$		$[Re(CO)_3(Zn-pyridyl-porphyrine)]_4$		$[Re_2(CO)_6(\mu\text{-bpy})(\mu,\mu\text{-bi-pyrimidine})]_2$	
	Mull.	vol.	Mull.	vol.	Mull.	vol.	Mull.	vol.
Re	1.23	2.9	1.17	2.58	−0.03	1.43	1.24	2.88
Zn					1.01	1.05		
Cl	−0.6	−0.3	−0.61	−0.33	−0.59	−0.41		
O	−0.74	0.08	−0.39	0.21	−0.82	0.23	−0.37	0.16
N_1					−1.29	−0.17	−0.86	−0.16
N_2	−1.22	−0.1	−0.83	−0.14	−1.25	−0.02	−0.89	−0.24
C_1[b]	0.55	−0.73	0.24	−0.74	0.91	−0.45	0.19	−0.72
C_2[c]			0.40−0.07−0.49		0.53	0.02	0.35	0.45
			0.01					
				0.53	0.03	0.41	−0.09	0.52
				0.14	0.17	0.41	−0.01	0.12
					−0.18	0.02	0.35	0.50
					0.24	0.34	−0.19	0.55
					0.02	0.49	0.72	−0.11
	0.71	0.45			0.81	0.40		

[a] A Fermi function roll-off with radius $1.2a_0$ was used to define overlapping atomic volumes for the purpose of integration. [b] Carbon atom in carbonyl group. [c] Carbon atoms on the bridging ligands. Multiple values represent sampling of inequivalent sites.

well-studied $[Ru^{II}(bpy)_3]^{2+}$ luminescent complexes. Such simplified pictures do not take into account further bonding interactions and charge transfer into and from the diffuse 6s and 6p orbitals; thus, more detailed analysis of the self-consistent charge distribution is required. Semiempirical molecular orbital (MO) models of mono- and binuclear Re(I) complexes suggest that the lowest unoccupied molecular orbital (LUMO) critical for redox interactions is a mixture of metal dπ within a formal π^* ligand MO.[18] Other semiempirical models used to interpret UV−vis absorption spectra also point to a complex interaction between metal-d and ligand-π character of critical MOs.[19]

The present first-principles calculations more clearly establish MO composition for further interpretations of both the ground state and the excitation properties. Stor et al.[20] reported DFT calculations of the complexes *fac*-$XMn(CO)_3$(bpy) (X = Cl, I) in a bidentate conformation similar to that of the Re−4,4′-bipyrimidine bonding. Here Mn is expected to be isoelectronic to Re; however, its 3d orbitals in the molecule may be expected to be more compact than those of Re 5d. They found a heavy contribution of halide character in the highest filled MO's, mixed with metal-d and carbonyl-π. The lowest excited states were predicted to be bpy π^*, followed by antibonding Mn−bpy and Mn−X states. This prediction of an active halide character in frontier MOs will be seen to be a common feature with the Re complexes.

2. Results. We find as expected that rhenium is an electron donor in the cornerpost unit and slightly more so in the molecular squares and rectangles, where electrons can be delocalized to the π system of bridging ligands. The net Mulliken charge on Re ranges from 1.97e (bpy rectangle) to 1.51e (bpy−Zn−por) in the compact basis (Table 1) and 1.24e and −0.03e respectively in the extended basis (Table 2). In the square formed by Zn−porphyrin as bridging ligand, the Re is least ionic, no doubt because the four Zn atoms are also electron donors, helping to saturate the π system.

The bond orders (units of e/bond) between the Cl, N, and C_1 (carbonyl) ligands of Re quantify the covalent part of the pairwise interactions. We find (basis B2) that the Re−C_1 bonding charge is greatest, ranging from 0.39 (bpy square) to 0.43 (pz square). The Re−N shared charge ranges from 0.23 (bpy square) to 0.12 (pz corner), the sum of C_1− and N− bond charges being roughly constant. The Re−Cl bond charge is roughly constant, ∼0.2 e/bond, with the bpy square in a puckered configuration (0.05) being the exception. While we might suppose that the Re−Cl bond is essentially ionic, these data show that the halide has a sizable covalent component, in some cases greater than that of Re−N. This is consistent with the calculated Mulliken charges: Cl (−0.30 to −0.61) versus N(−0.89 to −1.25). The bond order sequence for the bpy square is, thus, Re−C_1 (0.39) > Re−N (0.23) > Re−Cl (0.05).

Ratios of charge densities at the bond critical points are informative: taking the Re−C_1 (carbonyl) ρ_c as the reference value, we find for the bpy square Re−C_1 (1.0) > Re−N (0.51) > Re−Cl (0.44) and for the pz square Re−C_1 (1.0) > Re−N (0.56) > Re−Cl (0.54). Therefore, these bond orders and bond critical point charge densities give a consistent picture, which we expect will map onto relative bond strengths.

In the case of the Re cornerpost, the number of significantly participating MOs is sufficiently large that it is advantageous to analyze partial DOS, rather than focusing upon single MO composition. Re 5d bands are mainly seen in three regions. The lower valence band spanning from −10 eV to −5 eV contributes bonding stability by overlap with the carbonyl groups. The upper valence band, running from −5 eV to E_F, overlaps strongly with the Cl, N, and carbonyl orbitals. The excited states of the Re 5d bands, $E > E_F$,

(18) Page, S. E.; Flood, A.; Gordon, K. C. *J. Chem. Soc., Dalton Trans.* **2002**, 1180.
(19) Walters, K. A.; Premvardhan, L. L.; Liu, Y.; Peteanu, L. A.; Schanze, K. S. *Chem. Phys. Lett.* **2001**, *339*, 255.
(20) Stor, G. J.; Stufkens, D. J.; Vernooijs, P.; Baerends, E. J.; Fraanje, J.; Goubits, K. *Inorg. Chem.* **1995**, *34*, 1588.

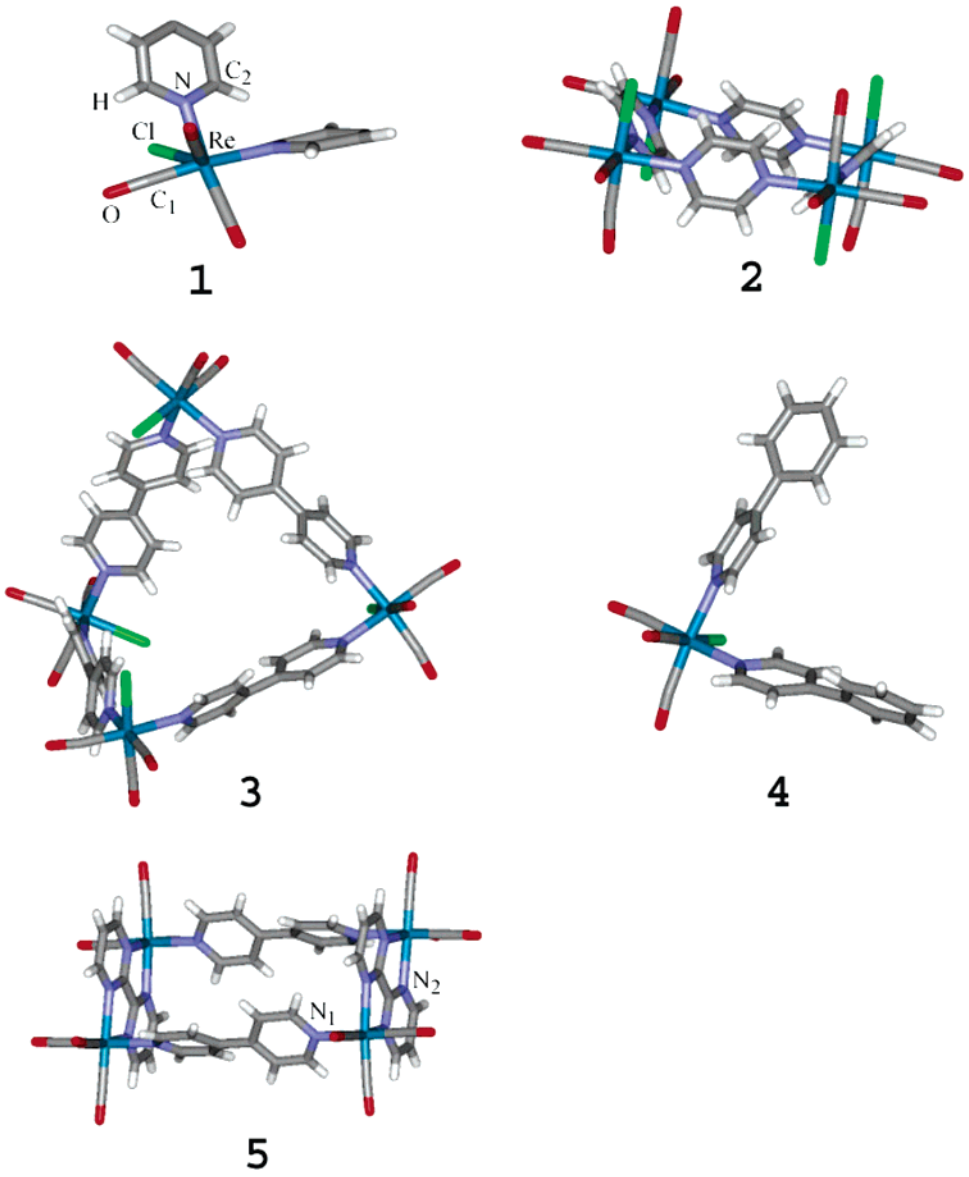

Figure 1. Stick diagrams showing wall orientation of the (1) pz corner and (2) pz square. Key atoms are enumerated as used in PDOS analysis. In the square, Cl ligands (green) are in alternating up−down configuration. (3) Configuration of the bpy square, showing the puckered conformation in the solid, in alternating up−down Cl isomer (green). Also shown (4) are the bpy corner and (5) bipy rectangle. All are taken from X-ray structures; see text.

appear in the IR−vis optical region beginning about 2 eV above E_F. By examining the PDOS of C and N on bridging ligands, we find that these components form broad spectra ranging from the upper valence region well into the UV−vis excitation region. A comparison of excited-state PDOS data with measured and calculated optical absorption is presented in a following paper.[21]

B. Pz Square and Corner. For the $[Re(CO)_3(\mu\text{-pz})Cl]_4$ molecular square,[6,22] see Figure 1, structure 2, the Re atomic configuration, according to (compact basis B1) Mulliken analysis, is $Re^{+1.65}$ $5s^{1.90}5p^{5.83}5d^{5.42}6s^{0.06}6p^{0.15}$. This is different from the neutral ground-state Re^0 $5s^25p^65d^56s^26p^0$, as a result of covalent bonding interaction with the ligands, including delocalization onto the bridging pz and charge transfer to CO and Cl and N atoms. The self-consistent Re configuration is also clearly more ionic than the nominal Re(I) invoked in simple electron-counting schemes for the Re complexes. Figure 2 shows a charge density map of the Re coordination environment in a plane containing Re and the two adjacent N. It reveals that the shared charge of the Re−C bond is large compared with the longer Re−N bond, consistent with bond-order charge analysis. Charges C_1 (carbonyl) and C_2 (pz) differ considerably between themselves and also differ according to results obtained by Mulliken population analysis (basis B1: 0.14, −0.24) and volume integration (−0.79, +0.46). This reflects not only the obvious differences between direct metal−C_1 bonding in carbonyl and the more distant ring−C interactions but also the rather diffuse nature of the carbon aromatic π electron system. As shown in the PDOS of Figure 3, the Cl valence 3p,4s contributions overlap strongly with occupied Re 5d states and dominate the region just below E_F. The pz carbon C_2 2p and nitrogen 2p states span 3−8 eV below E_F in the valence region. The pro-

(21) Ellis, D. E.; Miljacic, L.; Deng, B.; Snurr, R. Q.; O'Donnell, J. In preparation.

(22) (a) Belanger, S.; Hupp, J. T.; Stern, C. L.; Slone, R. V.; Watson, D. F.; Carrell, T. G. *J. Am. Chem. Soc.* **1999**, *121*, 557. (b) Slone, R. V.; Hupp, J. T.; Stern, C. L.; Albrecht-Schmitt, T. E. *Inorg. Chem.* **1996**, *35*, 4096.

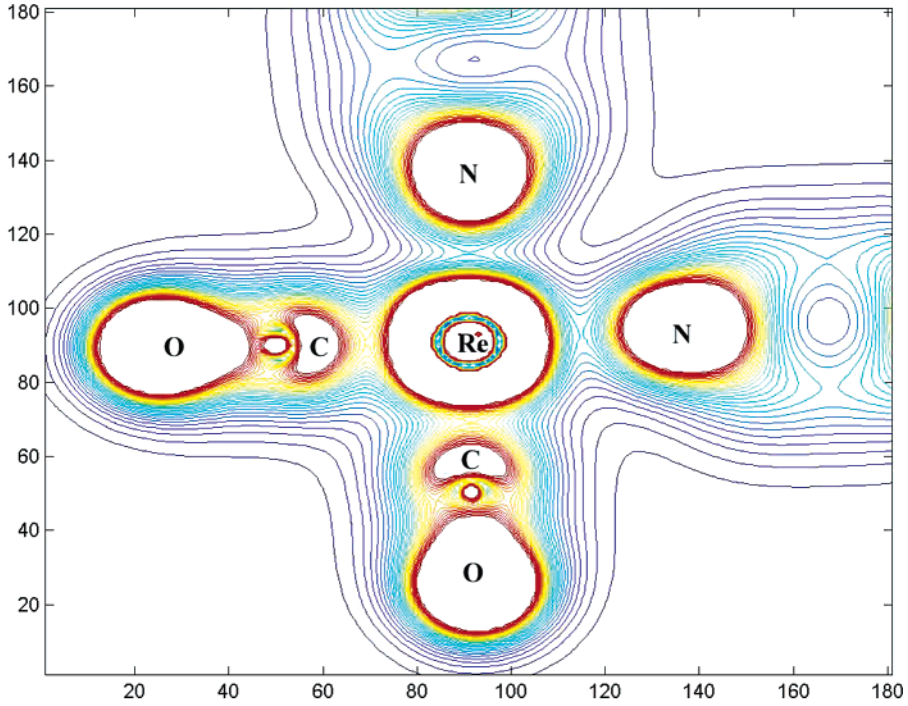

Figure 2. Charge density map of the Re−N−N plane of $[Re(CO)_3(\mu\text{-pz})Cl]_4$. Equal interval contours are shown.

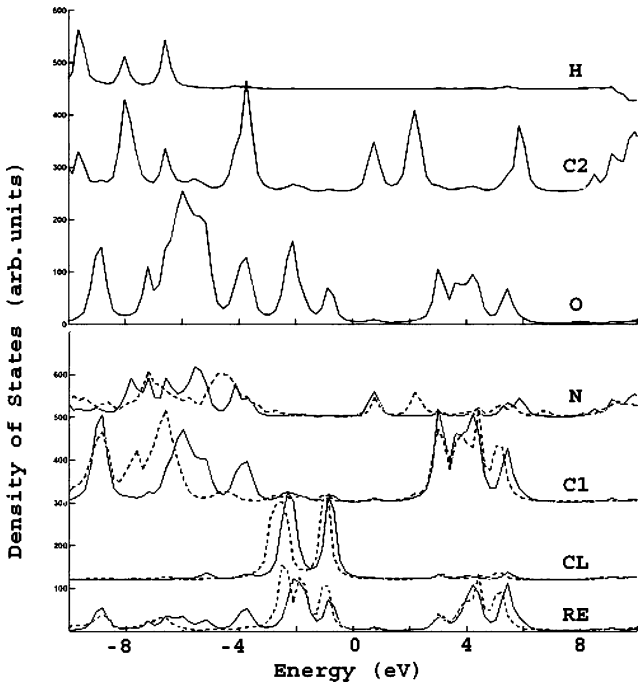

Figure 3. Partial DOS of the pz square (solid line): Re, Cl, C_1 (carbonyl), N, O, and C_2 (pz). For comparison, PDOS of selected atoms of bpy square are also shown (dashed line).

nounced N peak ∼1 eV above E_F gives rise to the first metal-to-ligand charge transfer bands, which we show[21] to be of low intensity. Re 5d also interacts with carbonyl C_1 2p states and oxygen 2p states ranging over 0−10 eV below E_F in the valence region.

The Re atomic configuration in the corresponding pz corner molecule $Re(CO)_3(\mu\text{-pz})_2Cl$[23,24] (see Figure 1, structure 1) according to Mulliken analysis is almost the same as the complete square, the Re charge being reduced by only 0.01e. The small difference calculated between the electron configuration in the square and that in the corner is surprising, because one might suppose that the change in the number of electron-withdrawing pz rings per Re atom would have a greater effect. This is evidence for the high degree of locality of the electronic distribution, which in turn is very useful for the "building-block" approach to synthesis and analysis of structural and reactive properties. The corresponding PDOS also reveal only small differences compared to the full square.

C. Bpy Square and Corner. For the $[Re(CO)_3(4,4'\text{-bpy})Cl]_4$ molecular square,[6,18] the metal atomic configuration in the observed puckered configuration is (basis B1) $Re^{+1.63}$ $5s^{1.91}5p^{5.85}5d^{5.43}6s^{0.07}6p^{0.12}$, which also differs little compared with the pz square discussed above. This indicates that substituting pz by bpy does not lead to significant changes in the electronic structure of the Re-related corner. Examination of the PDOS in Figure 3, dotted line, reveals some quantitative changes relative to the pz square; however, the main features of Re 5d states are very similar, with the occupied−unoccupied gap of ∼3 eV unchanged. The occupied bpy ring C_2 and nitrogen 2p states are shifted by ∼0.5 eV to greater binding compared to pz. The excited-state structure is very similar to that of pz.

In the molecular crystal, X-ray structural analysis shows (Figure 1, structure 3) that this "square" is highly distorted, with one unit nested within the other, and the dihedral angles between the least-squares planes of the pyridine rings are 37−38°.[22a] X-ray structural refinement of a disordered polymorph revealed a more nearly planar structure,[6] which we also calculated. Differences in atomic configurations and DOS between puckered and quasi-planar configurations were found to be rather small.

(23) Giordano, P. J.; Wrighton, M. S. *J. Am. Chem. Soc.* **1979**, *101*, 2888.
(24) Belanger, S.; Hupp, J. T.; Stern, C. L. *Acta Crystallog., Sect. C* **1998**, *54*, 1596.

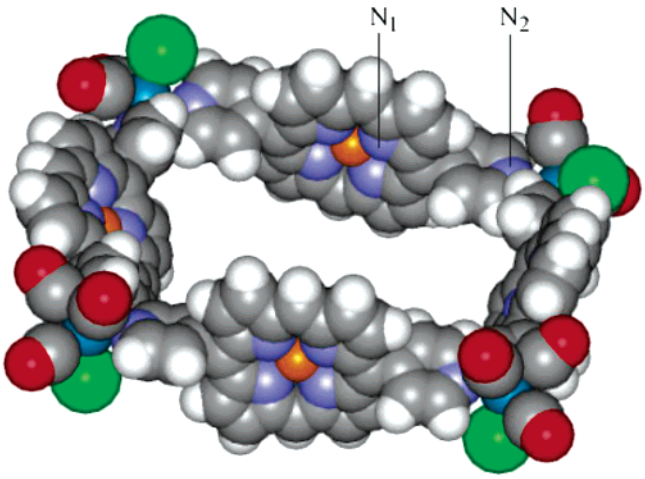

Figure 4. Model of the Zn porphyrin square, structure taken from molecular dynamics simulations[16] with modified Dreiding potentials.

The experimental configuration[22,26] of the bpy corner molecule is also shown in Figure 1, structure 4. The PDOS of the bpy corner are very similar to those of the bpy square, and the Re charge is reduced by only 0.02e, again demonstrating the high degree of superposition encountered in assembling the extended squares and rectangles.

D. Bpy Rectangle. For the $[Re_2(CO)_6(4,4'\text{-bpy})(4,4'\text{-bipyrimidine})]_2$ molecular rectangle,[26] Figure 1, structure 5, there are two kinds of bridging ligands, bpy and bipyrimidine, with resulting metal configuration $Re^{+1.97}\ 5s^{1.92}5p^{5.86}5d^{5.11}6s^{0.05}6p^{0.09}$. Because bipyrimidine is bidentate to Re, the metal can donate more electrons to bridging N ligands, which results in higher charge compared with pz- or bpy-based molecular squares.

The bpy rectangle Re, N_1, and C_1 PDOS features (not shown) are similar to those of the pz square. The absence of a chlorine ligand results in fewer states clustered just below the Fermi level, and substitution of Cl by N_2 (bipyrimidine) shifts the N excited state peaks to slightly lower energy. Re 5d states are also shifted to lower energy compared to those in the pz square, as a result of lack of Cl ligand; the C_1-(carbonyl) PDOS tracks with Re bonding features as expected. C_2 and oxygen 2p states are delocalized over the entire valence band.

E. Bpy−Zn−Por. The experimental compound, based upon the 2,8,12,18-tetrabutyl-3,7,13,17-tetramethyl-5,15-bis-(4-pyridyl)porphyrin, was simplified for calculations by replacement of tetrabutyl and tetramethyl terminal groups by hydrogen. The tetramethyl groups certainly have a strong effect on pyridyl−porphyrin rotational torsion constants, vide infra, but relatively small effects upon electronic structures in the ground configuration. When the bridging ligand is substituted as pyridyl zinc−porphyrin,[7] Figure 4, the Re atomic configuration is slightly less ionic compared with pz and bpy squares: $Re^{+1.51}\ 5s^{2.00}5p^{5.99}5d^{5.11}6s^{0.19}6p^{0.21}$. The Zn atomic configuration is (basis B1) $Zn^{+1.88}\ 3d^{9.85}4s^{0.12}4p^{0.15}$, close to the nominal divalent Zn^{2+} $d^{10}s^0$ values. SCF calculations were made on a 93-atom fragment consisting of one Zn−por wall and its two connecting Re−bpy cornerposts.

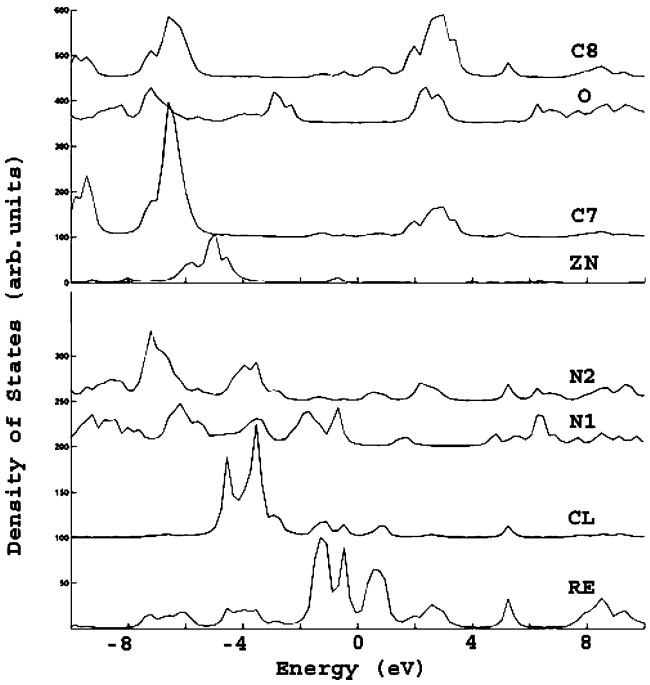

Figure 5. Partial DOS of the Zn−bpy−por square: Re, Cl, N_1, N_2, O, C_1, and C_2.

Re 5d states shift significantly toward the Fermi energy, forming a "metallic band" as shown in the PDOS of Figure 5. Oxygen 2p states are also affected by the bridging ligand substitution in that the bonding−antibonding gap widens to >4 eV, compared to ∼3 eV for nonbridged molecules. Prominent Cl 3p bonding states shift toward greater binding energy. Porphyrin C 2p and N 2p states form a strong band ∼1 eV above E_F, forming the final states of the well-known visible Q bands. Zn 3d states form a rather narrow band of ∼2 eV width, centered ∼5 eV below E_F, where strong hybridization with N 2p orbitals contributes bonding stability to the porphyrin.

IV. Conformational Properties and a Building-Block Approach

In our previous work, we have introduced the "piecewise" strategy in analyzing conformational properties of squares. We have shown that the largest Zn−por square can be suitably divided into smaller elements that carry the information about conformational preferences for the whole square. In this work, we have applied the same strategy on both the pz and the bpy squares. The most important geometrical parameters for the analysis are illustrated in Figure 6a, for the case of the bpy square. For more details on local geometries and the methodology, we refer the reader to ref. 16.

The pz square, with the shortest linking walls, is expected to exhibit the strongest coupling between rotations on successive sites and, thus, presents the most stringent test of a piecewise additive approach. The pz square was divided into cornerpost elements, each consisting of Re and its ligands, with pz rings rotated in parallel. During this

(25) Ortiz, T. P.; Marshall, J. A.; Emmert, L. A.; Yang, J.; Choi, W.; Costello, A. L.; Brozik, J. A. *Inorg. Chem.* **2004**, *43*, 132.
(26) (a) Benkstein, K. D.; Hupp, J. T.; Stern, C. L. *J. Am. Chem. Soc.* **1998**, *120*, 12982. (b) Benkstein, K. D.; Hupp, J. T.; Stern, C. L. *Angew. Chem., Int. Ed.* **2000**, *39*, 2891.

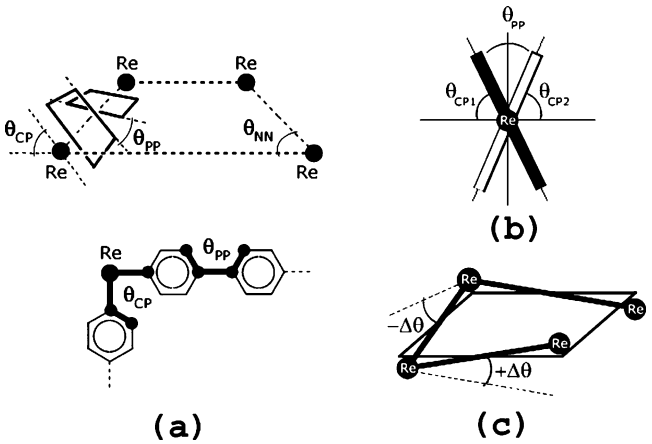

Figure 6. (a) Important geometrical parameters of the bpy square. The dihedral angle θ_{CP} between selected C, Re, and N atoms characterizes the rotation of a piridine ring respective to the square plane; the dihedral angle θ_{PP} connecting four C atoms of adjacent pyridine rings gives the relative angle between their planes; and θ_{NN} is the corner angle. (b) Edge-on view on two Re corners and a wall between, consisting of two rotating pyridine rings: the black one is closer to the viewer, and the white one is farther in the back, with ra elative angle between their planes θ_{PP}. (c) Small puckering introduces the dihedral Re−Re−Re−Re angle $\Delta\theta$, which two of the walls see as a positive shift in θ_{PP} and the other two see as negative.

procedure, a few selected degrees of freedom were allowed to relax: distance of rings to Re corner and two hydrogen atoms that have the most overlap with the opposite rotating ring. Torsional costs of this rotation were compared to the costs in total-energy calculations of the whole square, assembled a posteriori from partially relaxed element configurations. In thus assembled squares, walls are rotated in-out-in-out around the square, to mimic the experimental model, to minimize steric effects at cornerposts, and to increase the overall symmetry. The very good agreement between costs seen even for high energy configurations shows that the piecewise approach works even for the smallest of squares, which gives us confidence in the applicability of this strategy to the entire family of similar compounds.

As the first consequence, from the pz square, we see that a great deal of information about overall square conformation is contained in the cornerpost element. Turning now to the more extended bpy square, we note that the tendency of the N−Re−N angle θ_{NN} to be less than 90° leads to puckering of the square, and torsional costs to rotate the pyridine rings have the major influence on tilting of square walls. Next, we address both issues in more detail.

As described previously for the bpy−Zn−por system,[16] we have examined rotation of pyridine rings in parallel, while other Re ligands are kept fixed at perfect octahedral positions. As a next step, we repeat this procedure while allowing ligands to relax, with θ_{NN} fixed at 90°. These torsional costs are compared to the more restricted configuration in Figure 8, with curves shifted to zero for vertical rings. The main difference in geometry comes from bending of the chlorine ligand toward the rotating pyridine rings. As seen from the figure, this leads to a substantial reduction in costs and formation of a minimum when θ_{CP} is 55−60°. This is close to the experimental result for pz squares, whose walls are tilted 35−40° away from the vertical (90°) position. This minimum gives tilting of porphyrin walls to 30−40° away from the square plane, with a full-rotation barrier of less than

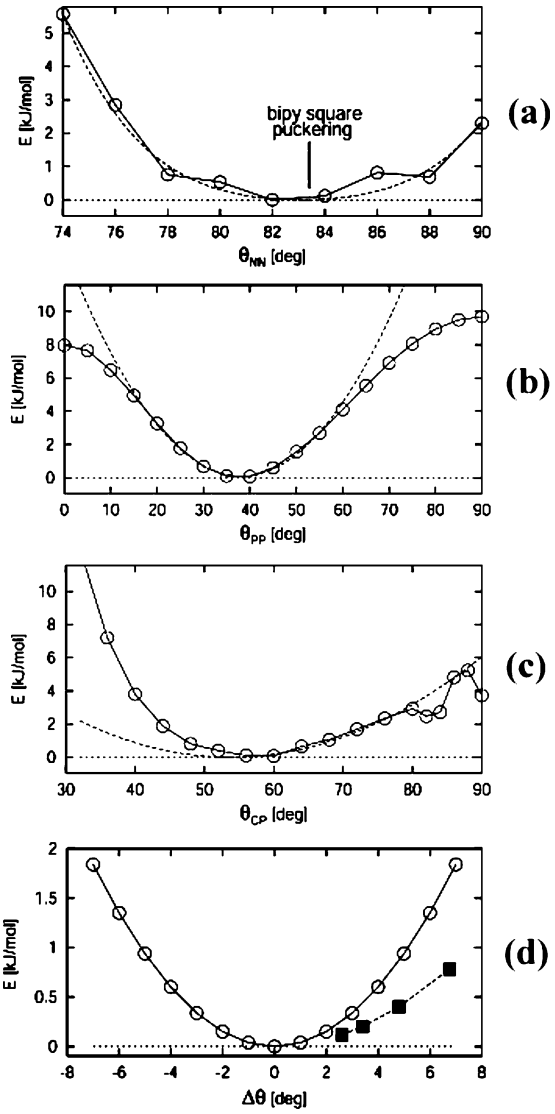

Figure 7. (a) Exploration of energy gain for the corner angle θ_{NN} less than 90°, which promotes puckering of the square; observed puckering angle of the bpy square is also shown. (b) Preference to relative orientation of the two adjacent pyridine rings of the bpy wall. (c) Torsional costs of rotating pz square walls, calculated by (○) summing contributions from four cornerpost elements. (d) The energy cost to slightly pucker the square (○) is higher than the corresponding gain (■). Dotted lines in (a−c) are the polynomial fits.

15 kJ/mol for a single wall. Thus, the walls posess a lot of torsional flexibility and can be strongly influenced by stacking interactions with walls of nearby squares.

Independent full geometry optimization of the cornerpost unit gave pyridine rings rotated at similar angles as in the observed structure. Therefore, we conclude that rotating rings in parallel, although representing a constrained motion, does lead to a configuration close to that of lowest energy. In the inset of Figure 8, Mulliken charge redistributions resulting from the rotation of the rings, with ligands relaxed, are shown for all the atoms of the unit, as a function of θ_{CP}. All charges are given relative to their values for vertical walls. We conclude that Re provides a small charge (about 0.06e) that can flow in and out of the carbonyl ligands, probably attracted by terminating hydrogens of rotating square walls. Finally, when θ_{CP} is 80−90° we observed some variations in the torsional curve of unclear origin. That this small barrier

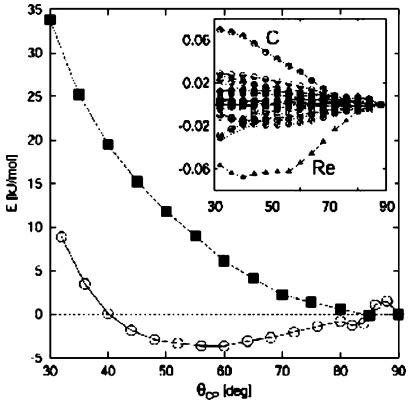

Figure 8. Comparison of energy costs of rotating in parallel two pyridine rings of the cornerpost element of the bpy square with Re ligands held fixed (■) and relaxed (○). In the more relaxed case, Cl bends toward the rings, significantly altering the torsion curve. The inset shows the charge redistribution (in units of [e]) of all the atoms present, following from this molecular motion. θ_{NN} is here fixed at 90°.

is not a computational artifact was verified by starting the relaxation process from either side of the maximum.

A planar square has four corner rheniums in the single plane, and $\theta_{NN} = 90°$. To deal with nonplanarity of squares, starting from the above-described minimal energy configuration, we have performed a series of cornerpost calculations for smaller θ_{NN}. All the Re ligands, the parallel rotation angle of the pyridine rings (θ_{CP}) and their distance to Re, and two most overlapping hydrogens were allowed to relax. As shown in Figure 7a, a minimum is seen at $\theta_{NN} = 82-84°$, which is in excellent agreement with experimental puckered conformation of the bpy square in the crystal $\theta_{NN} = 83.2-83.6°$. Thus, experimentally observed puckering in the crystal phase is not determined by the packing forces but is already present with the molecule in the vacuum. However, recent experiments[27] suggest that in the solution the puckering is, on average, half as great. A simple comparison of square energetics from Figure 7a,c with the thermal energy at room temperature ($k_BT \sim 2.5$ kJ/mol) shows that θ_{NN} can easily fluctuate between 76 and 90° and θ_{CP} can fluctuate between 40 and 80°. Therefore, the puckering and torsional forces are rather weak, and a considerable amount of angular disorder may be present in solution. Ortiz et al. argue that although the puckered conformation of the bpy square is the lowest in energy, the planar one is also stable, with an energy barrier between the two.[25] This suggests that squares in solution hop between the two configurations, thus bringing the average puckering angle closer to the measured value. We have applied the piecewise method to confirm this more clearly and to understand the origin of planar metastability.

Conformations of the bpy square are determined, in the piecewise method, by the costs of rotating two pyridine rings at the cornerpost (θ_{CP}) as shown in Figure 7c, and the cost of rotating the planes of the two bonded pyridine rings forming the wall one relative to another (θ_{PP}), as shown in Figure 7b. While rotating the two bonded rings, which stand for the "wall element" of the square, their mutual distance and two most overlapping hydrogens were allowed to relax. We have fitted the curves in Figure 7a−c in their respective regions of interest for this analysis with simple polynomials, as shown.

Figure 6b provides a schematic edge-on view of the two adjacent cornerposts with a wall in between. Two bonded pyridine rings forming the wall, the black (closer to viewer) and the white one (further behind), have their respective cornerpost angles θ_{CP1} and θ_{CP2}. The relative angle between their planes is $\theta_{PP} = (90° - \theta_{CP1}) + (90° - \theta_{CP2})$. The minimum energy conformation for the planar square is thus found from the fits, having θ_{PP} of about 49° and $\theta_{CP1} = \theta_{CP2}$ of about 69°, with all four walls/corners being symmetrical. We are interested in small perturbations $\Delta\theta$ of the dihedral Re−Re−Re−Re angle about the planar square, as shown in Figure 6c.

Puckering breaks the symmetry into two different pairs of walls. In the first approximation, small $\Delta\theta$ will simply shift two θ_{PP} of the whole square toward smaller and two toward higher values. We can, therefore, write the total torsional energy as the sum coming from two corners having θ_{CP1}, two having θ_{CP2}, and two pairs of intrawall interactions having shifts of opposite sign:

$$E(\theta_{CP1},\theta_{CP2}) = 2f_{CP}(\theta_{CP1}) + 2f_{CP}(\theta_{CP2}) + 2f_{PP}(\theta_{PP} + \Delta\theta) + 2f_{PP}(\theta_{PP} - \Delta\theta) \quad (2)$$

where $f_{CP}(x)$ and $f_{PP}(x)$ are simple polynomials, fitting curves of Figure 7b,c. The minimization of E with respect to θ_{CP1} and θ_{CP2} gives the energy cost of puckering the square for small $\Delta\theta$. Figure 7d compares this cost with the puckering benefit coming from contraction of the four corner angles θ_{NN}, as derived from a polynomial from Figure 7a. Indeed, the cost outweighs the benefit for small puckering. This result is not obvious because it comes from a delicate rivalry of two small effects. On one hand, each wall exerts a torque on the macrocycle; two pairs of torques oppose each other to restore planarity of the puckered square. On the other hand, the change in the corner angle $\Delta\theta_{NN}$ due to a small puckering $\Delta\theta$ is much smaller. The same push for planarity is present in pz and Zn−por squares as well, as follows from the asymmetry of the curve in Figure 7c around its minimum. In pz squares, a cornerpost pyridine ring is a square wall. In Zn−por squares, steric effects make the porphyrin perpendicular to its two neighboring pyridine rings, effectively locking the two into the same plane. The curve in Figure 7c, therefore, should contain all the information on the torques. Unfortunately, our data do not have enough precision to see whether other squares are stable in plane.

V. Concluding Discussion

The six molecules treated here show many common features derived from their Re cornerposts and pz, bpy, bipyrimidine, or Zn−porphyrin side walls. Self-consistent DFT calculations also present a coherent picture of the charge distribution and of contributions of distinct atomic orbital components to spectral features. In the ground state the nominal Re(I) configuration is significantly modified by covalent charge sharing with the ligands; 5d, 6s, and 6p diffuse orbitals participate actively in bond formation. In a compact NAO basis the Re net atomic charge ranges from

(27) O'Donnell, J. Private communication.

1.51 to 1.97e. The Re−Cl bond is found to have significant covalent character with implications for conformation control.

Analysis of conformational properties for this whole class of compounds can be greatly simplified by using a piecewise strategy, which is now shown to work well for both the largest and the smallest of the squares studied, despite noticeable differences among them in both charge densities and valence orbitals. Therefore, we are in the position to make several general statements about these macromolecules. As a common feature, the walls do not "see" one another across the square, except when they are artificially tilted into a near overlap, extending results of our previous work.[16] The isolated cornerpost unit alone contains the bulk of information on the conformational behavior of all squares and rectangles. This unit gives preference to specific orientation of walls, provides an energy barrier for their rotation, and leads to puckering of overall structure. We have found that softer Buckingham-type potentials better represent critical torsional interactions for use in MM simulations, compared to the initial Lennard-Jones scheme, at the cost of a greater number of parameters.

Rotation of pyridine cornerpost rings is strongly affected by the position of the negative chlorine ligand, which plays an unexpectedly significant role in orienting the walls. In retrospect, this could have been anticipated as a consequence of the considerable Cl covalent bonding component. If the relaxation of this ligand is taken into account, the full-rotation barrier for the walls in the Zn−por square is reduced by a factor of 5. This effect should be modeled in the future attempts to refine existing MM force fields. For future MM studies on this class of materials, a global reparametrization which better takes into account local torsions while maintaining general interatomic distances and vibrational structure would be desirable. Also, replacing chlorine with some other anion could have a strong role in modifying the overall geometry of squares and could be explored synthetically.

Metastability of the planar conformation comes from the torques asymmetric in $\Delta\theta$ that walls exert on nearby cornerposts, the effect being present in all the squares. However, we were only able to explicitly show that this is enough to give planar metastability in the case of the bpy square. The cornerpost energy dependence on θ_{CP} and θ_{NN} gives a good estimate of wall tilting of crystalline pz squares and correctly predicts puckering of the bpy square. The bpy square served as a good example to show that a piecewise strategy can not only facilitate calculations of larger systems but also provide insight beyond mere total-energy information.

The electronic density variations associated with wall rotation are fairly subtle, but they do lead to noticeable charge redistributions and shifts in absorption peak intensities.[28] These might be detected in sensitive optical experiments.

Acknowledgment. This work was supported by the National Science Foundation NIRT program, Grant CTS-0102612. The work of B.D. was supported by the NSF, through the MRSEC program at the Northwestern University Materials Research Center, Grant DMR-0076097.

(28) Miljacic, L.; Ellis, D. E. Unpublished results.

CM051214O